

Electrically Detected Magnetic Resonance in Dielectric Semiconductor Systems of Current Interest

P.M. Lenahan^a, C.J. Cochrane^a, J.P. Campbell^b, and J.T Ryan^b

^aPennsylvania State University, University Park, PA 16802

Email:pmlesm@engr.psu.edu

^bThe National Institute of Standards and Technology, Semiconductor Electronics Division, Gaithersburg, MD 20899

Several electrically detected magnetic resonance techniques provide insight into the physical and chemical structure of technologically significant deep level defects in solid state electronics. Spin dependent recombination is sensitive to deep level defects within semiconductors or at semiconductor dielectric interfaces. Spin dependent trap assisted tunneling can identify defects in dielectric films and, under some circumstances, can provide fairly precise information relating energy levels to physical/structural information about the defects under observation.

Introduction

The performance of solid state devices is inevitably affected by the presence of point defects with energy levels within semiconductor or insulator band gaps. Although many electrical measurements such as deep level transient spectroscopy, capacitance versus voltage, charge pumping, gated diode measurements, etc. can provide information about defect energy levels and densities, only electron paramagnetic resonance (EPR) offers the analytical power necessary to provide detailed structural and chemical information about the underlying point defect structures [1,2]. Unfortunately, conventional EPR sensitivity is about 10^{10} , a sensitivity too low for measurements in almost any fully processed solid state device. Conventional EPR also has the disadvantage that it is sensitive to all paramagnetic defects within a sample under study, whereas the active volume of a solid state device, for example metal-oxide-semiconductor field-effect-transistors (MOSFETs), is typically a very small fraction of the semiconductor substrate volume. Electrically detected magnetic resonance (EDMR) offers several significant advantages over conventional EPR in device physics studies [3-11]. The sensitivity of EDMR is at least seven orders of magnitude greater than that of conventional EPR [5-11]. EDMR is sensitive only to electrically active defects within the active area of the device under study [5-11]. EDMR can, at least crudely, provide information about both the spatial distribution and the energy levels of the defects under study.

Most EDMR studies to date have utilized spin dependent recombination (SDR). These measurements, like conventional EPR are sensitive to paramagnetic defects. Paramagnetic defects usually have an odd number of electrons, though under certain circumstances, paramagnetic EPR active defects with an even number of electrons may also be observed, for example defects with an electron spin of one. Both conventional EPR measurements and EDMR measurements involve the simultaneous application of a

large, slowly varying, magnetic field and a microwave frequency magnetic field. Resonance occurs when the microwave photon energy equals the Zeeman splitting energy of the electrons. In the simplest case, $h\nu = g\beta H$. In this expression, h is Planck's constant, ν is the microwave frequency, β is the Bohr magneton, and H is the magnetic field at resonance [1,2]. The g depends upon the relationship between the magnetic field vector and the orientation of the defect under observation. The behavior of g is expressed as a matrix sometimes called the g tensor [1,2]. The magnetic resonance condition becomes more complex when the paramagnetic site involves magnetic nuclei. The nuclear moment generates a local magnetic field which alters the magnetic resonance condition, depending on the nuclear spin quantum number, the magnitude of the nuclear moment, and the electron wave function [1,2]. The effect of a nuclear moment on the resonance condition is referred to as a hyperfine interaction [1,2]. Additional factors can also play a role in determining EPR spectra, for example, when multiple electrons are involved at a paramagnetic site, so called zero-field splitting or fine structure can also affect the EPR spectrum [1].

An analysis of EPR spectra utilizing the well developed understanding of these factors quite frequently allows the physical and structural nature of the defects under study to be identified. The atoms involved as well as electron wave function parameters are frequently elucidated from an analysis of EPR spectra. Since the EDMR spectra are very nearly identical to those of conventional EPR, this analytical power is also available in the EDMR measurement.

Most EDMR measurements have involved SDR. In SDR [3-11], one detects a magnetic resonance spectrum by measuring a change in device recombination current dominated or at least strongly influenced by recombination of electrons and holes at a deep level defect. The SDR effect can be understood in a qualitative way by considering the Shockley-Read-Hall model for recombination through deep level defects [3-11]. The process involves the capture of an electron and then a hole at a deep level center. The sequence can, of course, be reversed. It is difficult to envision such a process without the involvement of a paramagnetic charge carrier capture event at a paramagnetic deep level. The capture of a paramagnetic charge carrier at a paramagnetic defect is spin dependent. Consider a simple "dangling bond." If the dangling bond is occupied by an unpaired electron and then captures a conduction electron, the two electrons must have different spin quantum numbers. The recombination process must involve a singlet. This is so because of the Pauli exclusion principle. If the conduction electron and the deep-level defect electrons have the same spin quantum number, the process is forbidden. However, in the magnetic resonance process, the electron's spin is flipped from one quantum number to the other when the resonance condition is satisfied. Therefore, flipping the deep-level defect spin makes a previously forbidden transition allowed, thereby increasing the recombination current [3-11].

Lepine [3] was first to address potential models for SDR. He envisioned a process in which two spins interact essentially in an instantaneous collision; in his model, the size of the effect is limited by the product of the polarization of the two spin systems; that of a charge carrier and that of a paramagnetic deep level defect. For room temperature measurements involving simple defects, the product of the polarization of two spin systems would be approximately 10^{-6} at the widely utilized X-band frequencies and corresponding fields. This is so because the polarization of a system of very weakly

interacting electron spins, with g matrix components all close to 2, is approximately $g\beta HkT$, where β is the Bohr magneton, H is the magnetic field, k is Boltzmann's constant, and T is absolute temperature [1]. In such measurements, all the g matrix components are typically all close to 2, and the magnetic field at resonance is typically about 3400 Gauss. If we take room temperature to be 294 K, these parameters yield a polarization of about 1×10^{-3} for each of the spin systems and thus a product of about 1×10^{-6} . In a Lepine like process then, the maximum possible effect would be a current change of about one part in one million. Kaplan *et al.* [4] proposed an SDR model in which they envisioned a coupling between a pair of spins for a finite time. The model of Kaplan *et al.* [4] could be consistent with a much larger effect.

There are only a handful of reports of EDMR observations via spin dependent tunneling (SDT) in the literature [8-11] and very little in the way of detailed models; nevertheless, the fundamental concept is similar to that of SDR. The spin dependent tunneling event involves two spins. One might envision a conduction electron tunneling into a deep-level defect or tunneling from one paramagnetic deep-level defect to another paramagnetic deep-level defect. A tunneling event involving two unpaired electrons with the same spin quantum numbers will be forbidden. A tunneling event involving two unpaired electrons with different spin quantum numbers could be allowed. Thus, satisfying the resonance condition of a paramagnetic deep-level defect involved in the tunneling process should also be detectable, if one can measure a device current due to or partially due to trap-assisted tunneling through the defect in question.

These two EDMR techniques have been applied to a number of systems of interest in solid state electronics. This paper reviews several recent EDMR studies involving important metal-oxide-semiconductor (MOS) reliability problems, the negative bias temperature instability (NBTI) and stress induced leakage currents as well as new materials based MOS technology, specifically SiC based MOS technology. In these studies, EDMR measurements have been carried out in parallel with more conventional electronic measurements such as gate controlled diode (DCIV) and simple gate current versus gate voltage (I_G - V_G) measurements. The review illustrates the power of these EDMR techniques with regard to chemical and structural information as well as energy levels and physical location.

Spin Dependent Recombination and Interface/Near Interface Traps

SDR has been applied to several MOS systems [5-11]. A comparison of the SDR response in two of them, illustrates both the analytical power of the technique as well as the (as yet somewhat limited) capability of the technique to provide information about the spatial extent of specific defect centers. In the Si/SiO₂ MOS system, interface trapping is dominated by defect centers precisely at the semiconductor/dielectric interface. In the "new materials" SiC/SiO₂ MOS system, this is not necessarily the case.

The Negative Bias Temperature Instability in Si/SiO₂ Interface Traps

A Si/SiO₂ MOS problem of current interest involves an instability in p-channel MOSFETs (p-MOSFETS) which occurs when the devices are subjected to negative bias at moderately elevated temperatures [12]. The so called negative bias temperature instability (NBTI) is arguably the most important reliability problem in present day

conventional MOS technology. Recently, Campbell et al. [7,8] have explored the generation of interface trap generation due to NBTI in both conventional SiO₂ and nitride SiO₂ based MOS devices [7,8]. Some representative NBTI results are illustrated below for the case of a pure SiO₂ gate device. Negative bias temperature stress (NBTS) was applied to the 7.5 nm gate device at 140 °C for 250,000 s with -5.7 V on the gate contact. Both pre- and post-NBTS gate-controlled diode DCIV measurements on a device are shown in figure 1.

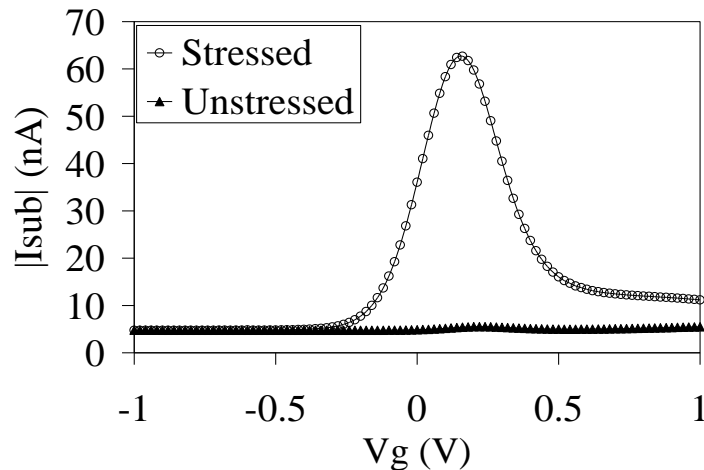


Figure 1: Gate-controlled diode DCIV measurements on a pMOSFET before and after the application of NBTS (140 °C for 250,000 s with -5.7 V on the gate contact).

In the gate-controlled diode DCIV measurement, the source and drain are shorted, the source/drain to substrate diode is slightly forward biased (0.33 V in these measurements) and the source/drain to substrate recombination current is monitored as a function of gate bias. Fitzgerald and Grove [13] found that, if the deep level defects are all or nearly all at the semiconductor dielectric interface, a peak appears in recombination current at the biasing condition which yields equal densities of conduction electrons and holes at the semiconductor dielectric interface. This peak is characterized by ΔI_{sub} (difference between the peak and the baseline) which scales with the interface state density (D_{it}) and can be approximated by:

$$\Delta I_{\text{sub}} = (1/2) q n_i \sigma_s v_{\text{th}} D_{\text{it}} A q / V_F / \exp(q/V_F / / 2kT) \quad (1)$$

where q is the electronic charge, n_i is the intrinsic number of carriers, σ_s is the geometric mean of the electron and hole capture cross section, v_{th} is the thermal velocity, A is the effective gate lateral area, V_F is the forward bias applied to the source/drain to substrate junction, k is Boltzmann's constant, and T is the temperature. The change in recombination current (ΔI_{sub}) is proportional to the interface state density within an energy window $1/2 q/V_F$ [13]. These results illustrate all known observations that NBTS induces a large increase in the interface state density. Following the analysis of Fitzgerald and Grove [13], D_{it} values were extracted for pre-NBTS ($9 \times 10^9 \text{ cm}^{-2} \text{ eV}^{-1}$) and post-NBTS ($7 \times 10^{11} \text{ cm}^{-2} \text{ eV}^{-1}$), taking the mean capture cross section $\sigma_s = 1.4 \times 10^{-16} \text{ cm}^2$.

Figure 2 illustrates the corresponding pre- and post-NBTS SDR traces with the magnetic field vector perpendicular to the (100) surface. The interface defect density in the

unstressed device is below the Campbell et al. SDR detection limit. After NBTS, two strong signals appear at $g = 2.0057 \pm 0.0003$ and at $g = 2.0031 \pm 0.0003$ (figure 2). They attribute the $g = 2.0057$ signal to P_{b0} centers and the $g = 2.0031$ signal to P_{b1} centers. P_{b0} and P_{b1} defects are both silicon dangling bond defects in which the central silicon atom is back-bonded to three other silicon atoms precisely at the Si/SiO₂ boundary [2,6,14-16].

Figures 3 and 4 show schematic drawings of P_{b0} and P_{b1} centers. The P_{b0} center structure is well understood; the P_{b1} drawing should be viewed as, at best, a provisional sketch. The main differences between the two defects are in the dangling bond axes of symmetry [2,6,14-16] and electronic density of states [17-20]. The P_{b0} dangling-bond orbital points along the [111] directions, while the P_{b1} dangling-bond orbital points along the [211] directions. Both the (111) Si P_b center and (100) Si analog, the P_{b0} center, have a broadly peaked density of states centered about midgap with the (+/0) and (0/-) transitions separated by about 0.7 eV [17-20]. The P_{b1} density of states is much narrower and is skewed towards the lower part of the silicon band gap [17].

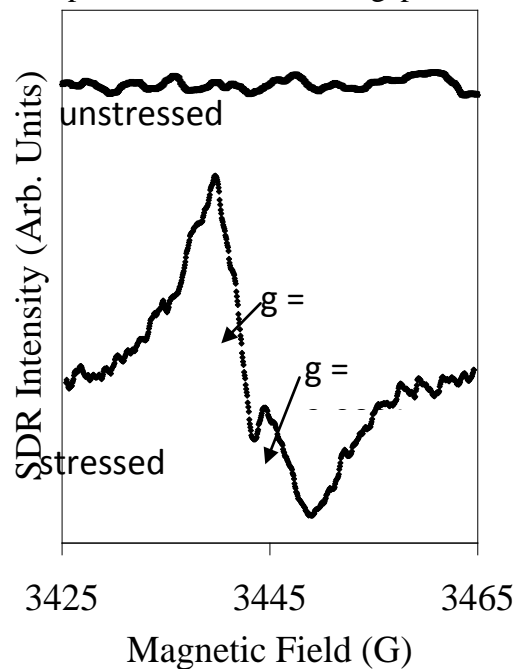


Figure 2: SDR traces of a pMOSFET with the magnetic field vector perpendicular to the (100) surface both before and after the application of NBTS (140 °C for 250,000 s with -5.7 V on the gate contact).

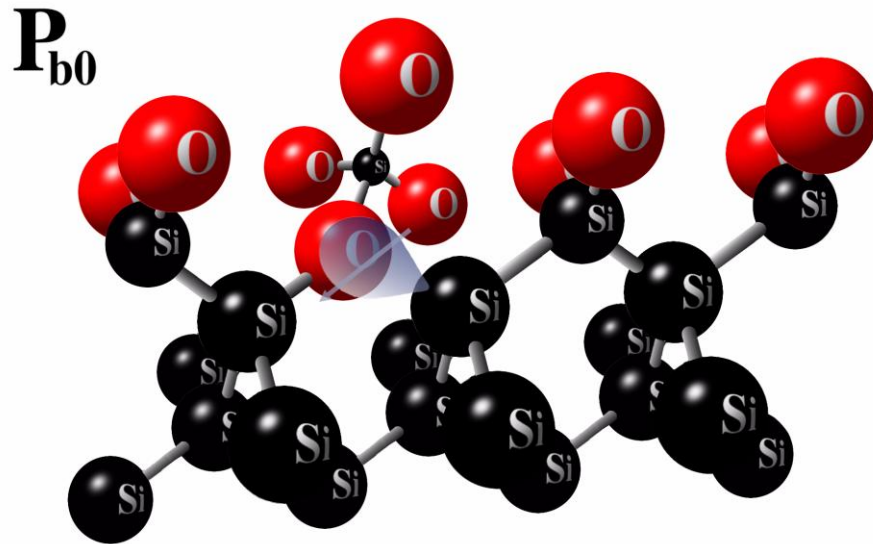


Figure 3: Schematic drawing of the P_{b0} Si/SiO₂ interface defect.

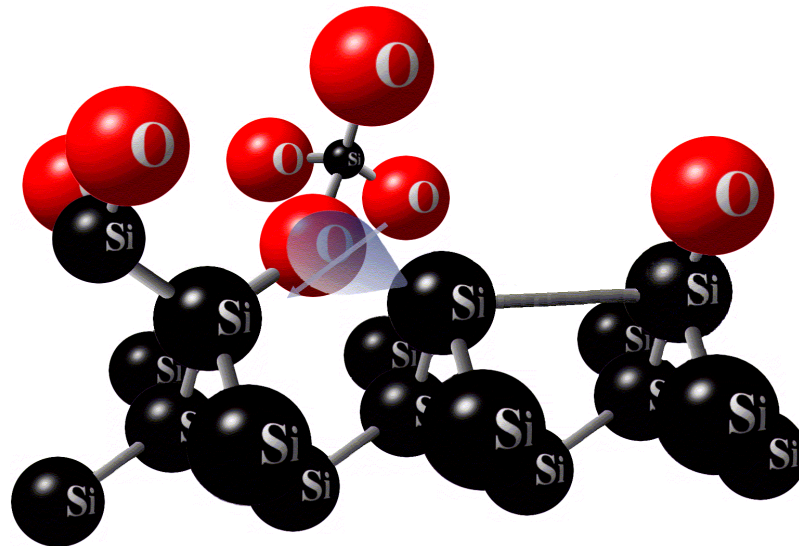


Figure 4: Schematic drawing of the P_{b1} Si/SiO₂ interface defect. It should be noted that this drawing in particular should be viewed as a cartoon which merely indicates that P_{b1} involves a silicon atom back-bonded to three other silicons at the interface.

Figure 5 illustrates the P_{b0} and P_{b1} SDR signal amplitudes as a function of gate bias for the same pMOSFET that was subjected to 140 °C for 250,000 s with -5.7 V on the gate contact. The dashed lines in figure 5 are only a guide for the eye. Note that both curves are strongly peaked, indicating that both P_{b0} and P_{b1} centers must be present at a single

plane, in this case, that of the Si/SiO₂ interface. The fact that these amplitudes are large only when the quasi-Fermi levels are close to symmetrically split about the interface intrinsic energy level is strong evidence for this physical location.

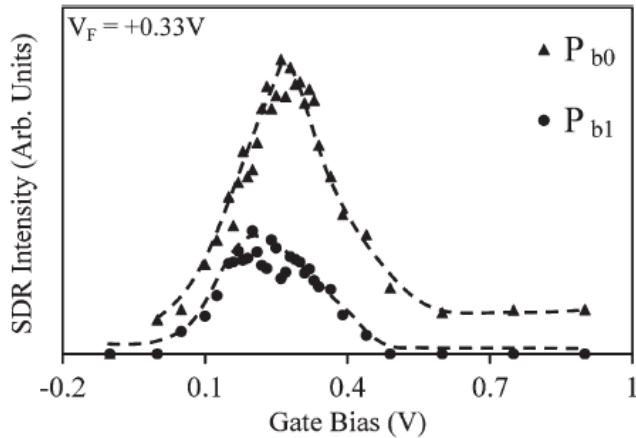


Figure 5: SDR-derived P_{b0} and P_{b1} signal amplitudes as a function of applied gate bias for the pMOSFET which had been subjected to NBTS (140 °C for 250,000 s with -5.7 V on the gate contact). The dashed lines are included as merely a guide for the eye. In these measurements, the magnetic field vector is perpendicular to the (100) surface.

These recent SDR results of Campbell et al. involve defects which are precisely located at a semiconductor/dielectric boundary. The strongly peaked SDR response corresponding to equal numbers of electrons and holes at the Si/SiO₂ boundary is strong evidence for this location (It should be noted that this location may be inferred from other results as well [2]). Recent EDMR results of Cochrane on a “new materials” based MOS system, that of SiC/SiO₂ yield a somewhat different conclusion regarding defect location. A comparison of the results of Cochrane et al. and those of Campbell et al. illustrate the (so far limited and qualitative/semi-quantitative) capability of SDR to provide information about the spatial distribution of electrically active defects.

Interface/Near Interface Traps in SiC/SiO₂ MOS Systems

Quite recently, Cochrane et al. [9] reported on a fairly extensive EDMR study of SiC based MOS systems. This study is of general interest for several reasons, among them, the potential of SiC based MOS technology and, more broadly, the materials physics issues of compound semiconductor based MOS technology. There is growing interest in MOSFETs composed of materials other than the classical Si/SiO₂ chemistry. Among the new material systems, SiC/SiO₂ is perhaps the most promising. SiC offers great promise for MOSFETs in high-power and high-temperature applications [21]. Unfortunately, these devices are plagued with performance limiting defects which are frequently viewed primarily as interface traps. It is often explicitly or implicitly assumed that these traps exist essentially right at the SiC/SiO₂ boundary and some recent studies suggest that the traps are quite similar to those which dominate the classical Si/SiO₂ system, semiconductor/insulator interface “dangling bond” centers [22]. Several fundamental questions about these defects have yet to be resolved. (1) What is the physical and chemical nature of the trapping centers? (2) Do these traps have a consistently defined

physical location, for example, the semiconductor/ insulator interface? (3) Do these traps have a common origin in all or nearly all SiC/SiO₂ structures? This is so in the Si/SiO₂ case.

Cochrane et al. [9] found a variety of SDR responses, which were extremely dependent upon device processing. Their study involved SiC lateral n-channel MOSFETs with gate areas of 100µm x 100µm. The devices all had essentially the same geometry. All were n-channel lateral MOSFETs with 50 nm to 70 nm gate dielectrics and 10⁴ µm² gate areas. In the representative results illustrated herein, all transistors were doped during epitaxial growth of the silicon carbide.

Figure 6 illustrates EDMR results on a 4H-SiC device with an entirely deposited oxide. Figure 6(a) illustrates a narrow EDMR scan and figure 6(b) a wider scan. A gate bias of 4 V was applied during the measurement. The traces illustrate a single strong central line accompanied by much weaker side peaks. This line has an anisotropic g, with $g_{\parallel} = 2.0026 \pm 0.0002$ and $g_{\perp} = 2.0010 \pm 0.0002$. This anisotropy is illustrated in the g-map of figure 7. The symmetry axis is, within experimental error, the crystalline c-axis, which is very close to the SiC/SiO₂ surface normal.

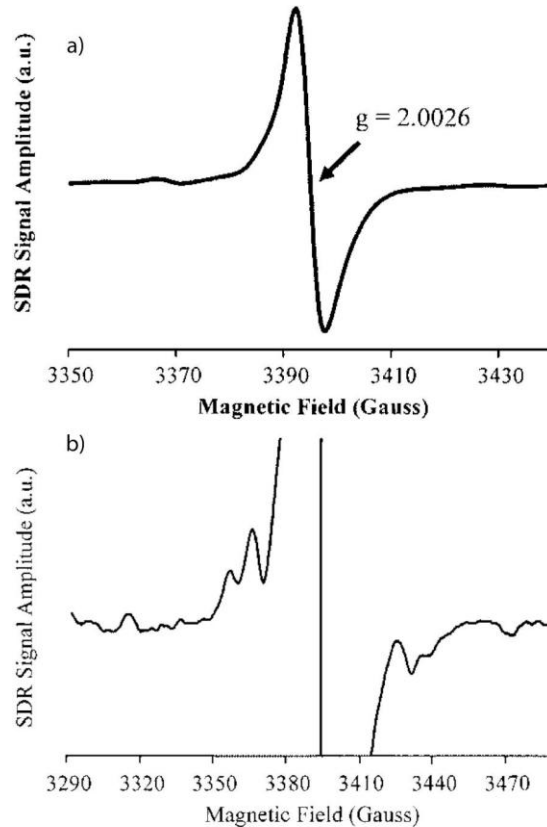


Figure 6: Narrow (a) and wider (b) scan EDMR traces taken on a deposited gate dielectric 4H-SiC MOSFET configured as a gated diode. The magnetic field is approximately parallel to the crystalline c-axis and also very nearly parallel to the SiC/SiO₂ interface normal. The traces show a strong central line; at this orientation $g_{\parallel} = 2.0026 \pm 0.0002$.

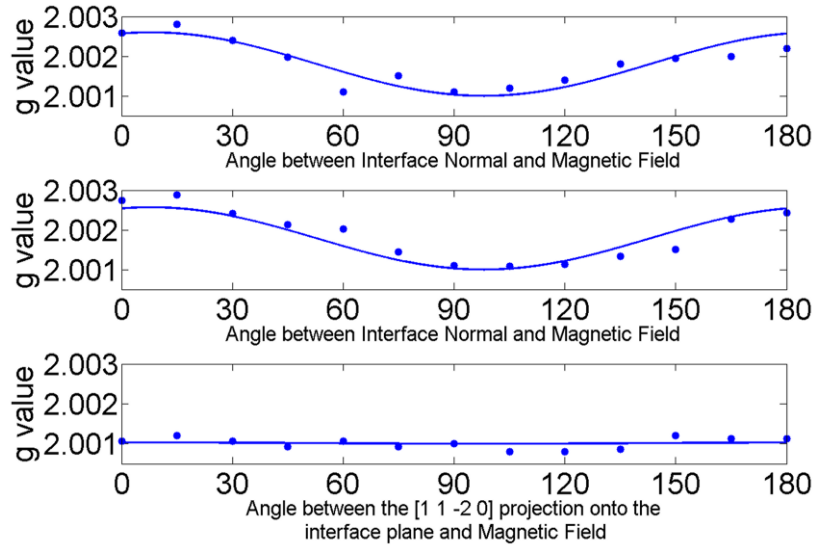


Figure 7: The g vs. magnetic field orientation with respect to the surface normal rotation about the three perpendicular axes. (a) This axis corresponds approximately to the $[112\bar{0}]$ axis and the surface normal is 8° from the $[0001]$ crystalline axis. (b) The g vs. magnetic field orientation with respect to the surface normal rotation about the integrated circuit side edge axis. This axis corresponds approximately to the $[11\bar{0}0]$ axis. (c) The g vs. magnetic field orientation with respect to the edge axis of the integrated circuit for rotation around the surface normal. Note: the solid lines correspond to calculated g values utilizing the correct crystalline orientation and $g_{\parallel}=2.0026$ and $g_{\perp}=2.0010$.

Elementary magnetic resonance theory [1,2] predicts that simple “dangling bond” defects with an unpaired electron primarily localized on one p-character orbital on an atom with zero nuclear spin would yield a magnetic resonance spectrum consistent with the results of figures 6 and 7. (About 95% of silicon nuclei possess zero nuclear spin.) Simple theory [1,2] predict that the resonance g matrix would be axially symmetric with the axis of symmetry of the high p character orbital. Theory also predicts that the g corresponding to this orientation would be $g_{\parallel} \approx 2.0023$. The largest deviation from this value would occur when the magnetic field perpendicular to the symmetry axis, this would be g_{\perp} [1,2]. A simple “ball and stick” model at the SiC/SiO₂ interface does indicate the possible presence of dangling bond defects with symmetry axes corresponding very nearly to the SiC/SiO₂ interface normal. If these spectra came only from conventional EPR, one might erroneously conclude that the observed defects are all SiC/SiO₂ interface dangling bonds much like the Si/SiO₂ P_b centers. However, as mentioned previously, SDR can provide some information about the physical distribution of defects.

Figure 8 illustrates DCIV and EDMR amplitudes versus gate voltage from the transistor utilized in figures 6 and 7, a 4H-SiC device with a deposited oxide/nitride/oxide dielectric 50 nm thick. Figure 8(a) illustrates the EDMR amplitude as a function of gate bias and figure 8(b) illustrates the recombination current, that is, the DCIV measurement as a function of gate bias. Both responses are peaked near zero volts, though the DCIV peak is rather weak. Under this biasing condition, the SiC/SiO₂ interface region is depleted. As the analysis of Grove and co-workers [13] indicates, at modest junction forward biases,

2.15 V in this case, the current is dominated by recombination in the depletion region. With a gate bias which provides equal numbers of electrons and holes at the location of the highest density of deep levels, the recombination current will peak [13]. This is so because, if nearly all the deep-level defects responsible for recombination are at a specific location, the recombination current will be maximized if equal densities of electrons and holes are present there [13]. In the Si/SiO₂ system, this location is invariably the Si/SiO₂ interface. If the SiC device had a physical distribution of defects similar to that of a silicon device (near perfect bulk semiconductor, deep-level defects predominately at the semiconductor/dielectric boundary) the EDMR amplitude would be expected to exhibit a fairly strong peak but only a very weak peak is evident in the DCIV curve. This indicates that, in these devices, there is not a particularly predominant density of defects at a specific plane within the device (the SiC/SiO₂ interface) but a broader distribution; so the result indicates a moderately high density of deep-level defects at the SiC/SiO₂ boundary (thus the weak peak) but that high densities extend into the “bulk” of the SiC epilayer. The overall similarity between the DCIV and EDMR curves suggests that the defects observed in magnetic resonance are the dominating deep levels in this device

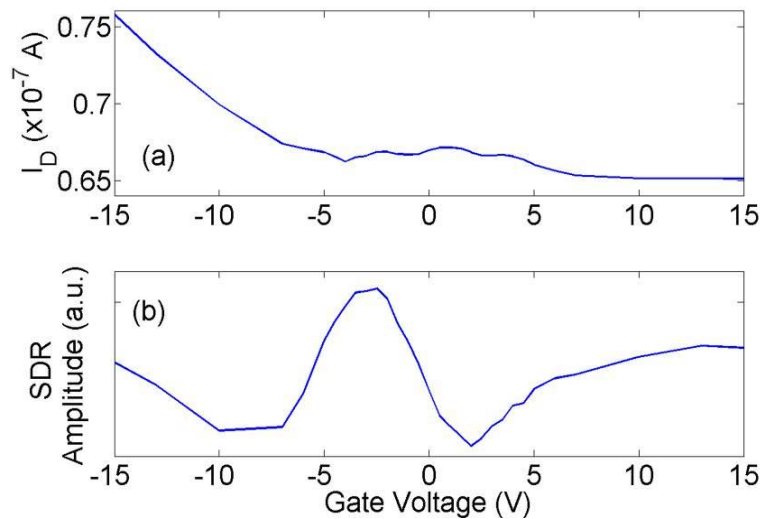


Figure 8: DCIV (a) and EDMR (b) amplitude vs. gate voltage for the 4H-SiC transistor utilized in figures 6 and 7.

Figure 9 illustrates EDMR results on a MOSFET built on a 6H-SiC substrate. Figure 9(a) illustrates a narrow EDMR scan and figure 9(b) illustrates a wider scan. A gate bias of 5 V was applied during the measurement. In this case the strong central line has an isotropic g ; $g=2.0026 \pm 0.0002$. In these traces, strong but poorly resolved side peaks appear symmetrically located about the central line separated by about 15 G. Much weaker peaks are also present with a separation of about 60 G to 70 G.

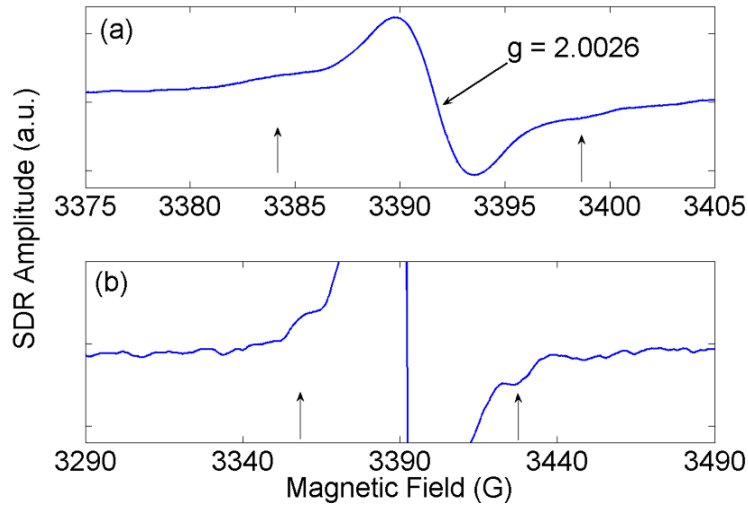


Figure 9: Narrow (a) and wider (b) scan EDMR traces taken on sample B, a thermal oxide/silicon nitride/thermal oxide gate 6H-SiC MOSFET configured as a gated diode. The magnetic field is approximately parallel to the crystalline c-axis and is also very nearly parallel to the SiC/SiO₂ interface normal. The traces show a strong central line with $g=2.0026 \pm 0.002$ and strong but poorly resolved side peaks separated by 14 G and much weaker and more distant side peaks separated by 60 G to 70 G.

The results of figure 9, a strong central line accompanied by strong (through poorly resolved) side peaks near the center line and much weaker more distant side peaks can be interpreted [9] in terms of a silicon vacancy. As discussed in some detail by Cochrane et al. [9] such a pattern is qualitatively consistent with both extensive conventional EPR literature on large volume samples [23,24] and a rudimentary analysis of the silicon vacancy defect structure [9]. A cartoon model of a silicon vacancy is provided in figure 10. (It should be noted that the correspondence between the conventional EPR spectrum reported for this defect and the SDR/EDMR results are only qualitative. [9,23,24] It is conceivable that the assignment of Cochrane et al. is in error but the fact that the SDR results involve measurements in a highly defective SiC/SiO₂ interface region may plausibly account for the differences.)

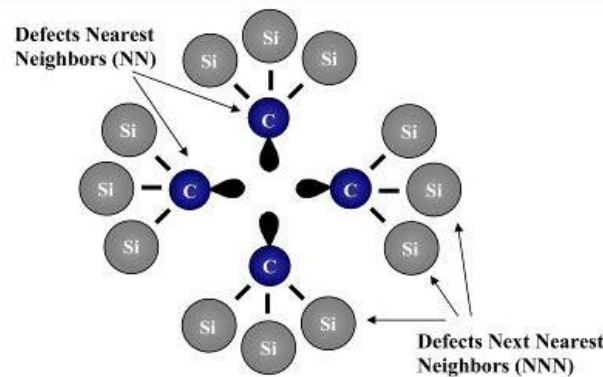


Figure 10: A cartoon schematic of a silicon vacancy in SiC.

Figure 11 illustrates DCIV and EDMR amplitudes versus gate voltage from the transistors utilized in figure 9, a device with a 50 nm thermal oxide on 6H-SiC. Figure 11(a) illustrates the EDMR amplitude as a function of gate bias and figure 11(b) illustrates the recombination current (DCIV) versus gate bias. Note that both the EDMR and DCIV responses are significantly different from the results of figure 8. In this case, the EDMR and DCIV amplitudes are quite strongly peaked at modest gate bias; EDMR signals virtually disappear at large positive and negative voltages. These results indicate that, in this device, there is a specific plane (the SiC/SiO₂ interface) at which the deep-level defect density is much higher than in the near-interface SiC. The fairly close similarity between the DCIV and EDMR suggest that, in this device, the defects observed in magnetic resonance are largely responsible for the dominating deep levels.

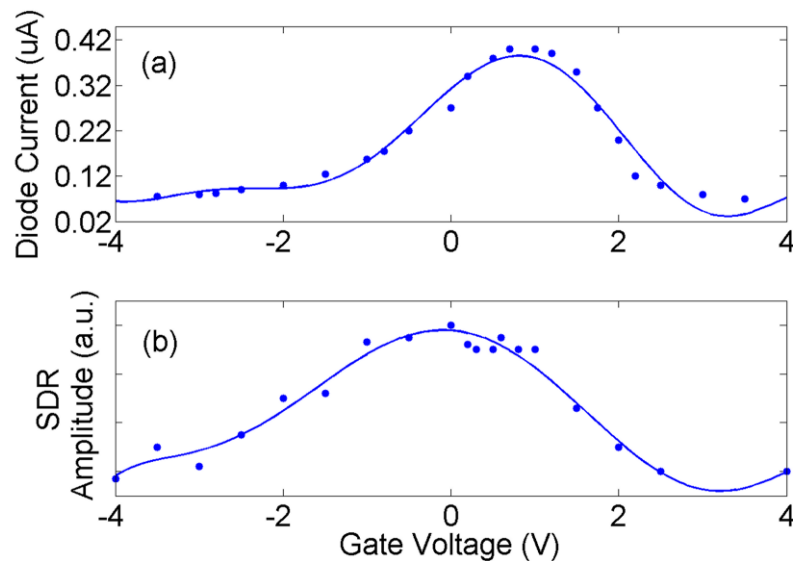


Figure 11: DCIV (a) and SDR (b) amplitude vs. gate voltage for the 6H-SiC sample utilized in figure 9. Note the qualitative correspondence between the SDR and DCIV responses.

The Utility of EDMR/SDR in Providing Information About Defect Location

The results just discussed show that SDR results in Si/SiO₂ systems and SiC/SiO₂ systems are quite significantly different. The differences provide useful information. In MOSFETs based on the Si/SiO₂ system, as the representative results of Campbell illustrate, and as other results in the literature not shown here also illustrate [2,5,6] the electrically active defects of interest are truly INTERFACE traps. This is indicated by the strongly peaked SDR response and the strongly peaked DCIV response. The dominating defects must be primarily present at a plane, the semiconductor/dielectric interface. Strong clues supporting this conclusion are also provided by the magnetic resonance spectrum itself [2]. In MOSFETs based on SiC/SiO₂ systems, the SDR and DCIV response does not necessarily have this simple peaked structure, indicating a more complex system of interface/ near interface trapping defects. The magnetic resonance spectra are also somewhat more complex with significant differences appearing in differently processed devices and in devices prepared on different polytypes.

Energy Resolved Spin Dependent Trap Assisted Tunneling in Very Thin Dielectrics

Recently Ryan et al. [10,11] reported on a very simple approach to spin dependent trap assisted tunneling (SDT) which allows for the evaluation of the energy levels of traps in thin dielectric films. The approach exploits advantages provided by extremely thin 1.2 nm effective oxide thickness (EOT) dielectrics. The enormous difference between the very high capacitance of the thin dielectric and the much lower capacitance of the Si depletion layer allows a modest applied voltage to sweep through most of the Si band gap with very little net potential drop across the dielectric. The approach yields direct information about defect energy levels and provides magnetic resonance spectra with excellent sensitivity. The dielectrics utilized in their recent study were silicon oxynitride films quite widely utilized in essentially “state of the art” complementary metal oxide silicon (CMOS) integrated circuits. Deep level defects were generated within these films by subjecting them to high electric fields. The defect generating conditions were chosen because they represent the circumstances under which an important instability in present day CMOS integrated circuits occurs: stress induced leakage current (SILC) [25,26] They showed that SDT can be utilized to extract information about the electronic levels of dominating point defects generated by the stressing of this system. The approach is almost certainly widely applicable to the study of other important defects. The SDT samples utilized in their study were 1.2 nm EOT nitrided SiO₂ p-channel MOS capacitors with p+ poly-Si gates. The very high p+ doping of the gate effectively pins the gate Fermi energy (E_F) very close to the gate Si valence band edge (VBE). The gate areas were 10⁴ μm². Deep level defects were generated in the dielectrics by room temperature stressing of 2.2 V for 10⁴ s.

Figure 12 illustrates a normalized tunneling current, a ratio of tunneling current measurements taken before and after stressing, which emphasizes the contribution of the (stress induced) trap assisted tunneling component in the total current. Here, J_0 is the gate current density pre-stress and ΔJ is the gate current density post-stress (J_1) minus J_0 . The $\Delta J/J_0$ versus V_G plot illustrates the difference between the I_G - V_G curves before and after stress due to trap assisted tunneling current in the post-stress I_G - V_G measurement. The peak of this curve (around $V_G = 0.35$ V) corresponds to the maximum fractional contribution of trap assisted tunneling current, not the maximum total current. This is so because the total current is the sum of the trap assisted current and all other sources of current. The only other significant source of current in these very thin dielectrics, direct tunneling, is exponentially increasing with voltage. At higher voltages the current is dominated by direct band to band tunneling which overwhelms the trap assisted tunneling current. Values for $\Delta J/J_0$ around $V_G = 0$ V are not included because the amplitude of the currents are below the detection limit of the I_G - V_G measurements.

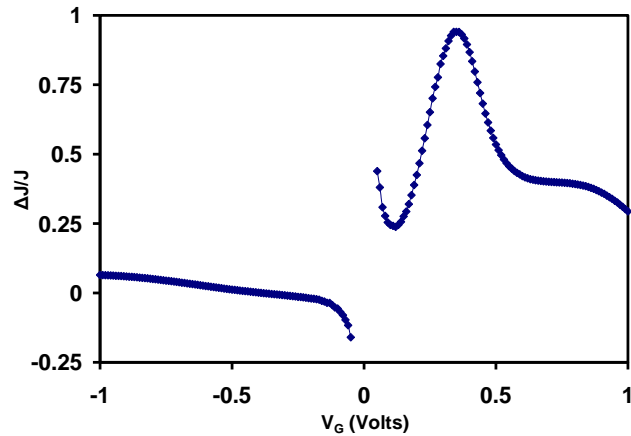


Figure 12: $\Delta J/J$ vs. V_G . The peak in the curve is caused by a trap assisted tunneling current in the stressed I_G - V_G measurement.

Figure 13 illustrates a representative SDT measurement taken with V_G biased to correspond to the peak in the $\Delta J/J_0$ curve of figure 12 ($V_G = 0.35$ V). In this figure, the measurement was made with the Si/dielectric interface normal parallel to the applied magnetic field (0°). The spectrum is a single line with a g of 2.0030 ± 0.0002 and a line width of about 15 G. The spectrum does not change when the sample is rotated; this very strongly suggests that the defects are located in an amorphous material. If the defects existed at specific orientations, as they would in a crystalline environment or were precisely at the Si/dielectric interface, the g value would almost certainly change as the sample is rotated in the magnetic field. For example, as discussed earlier in this paper, the g values of the dominating interface defects in conventional Si/SiO₂, P_b centers, change considerably as the sample is rotated in the magnetic field. The defects observed in this study do not follow such a pattern, ruling out a direct role for Si/dielectric P_b centers in the spin dependent trap assisted tunneling process. The magnetic field orientation independence, the zero crossing g value of 2.0030, and the 15 G line width of the observed defect spectrum are all consistent with the K center found in Si₃N₄ and some SiO_xN_y films [27-29].

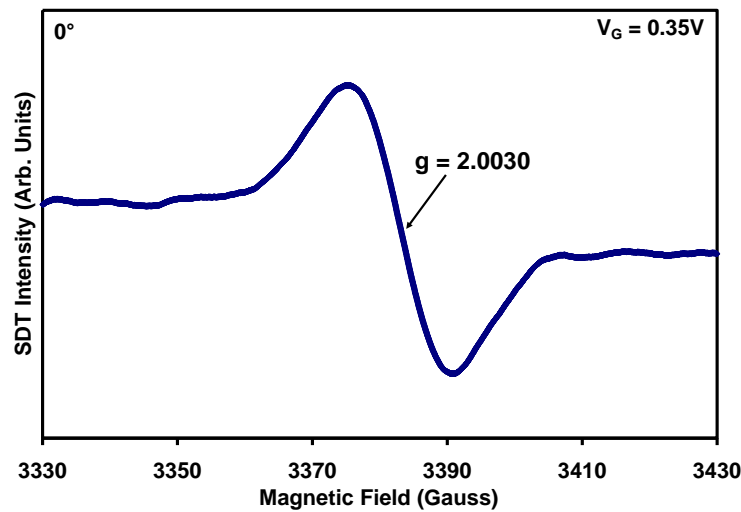


Figure 13: Representative SDT measurement taken with the gate biased to correspond to the peak in the $\Delta J/J$ curve of figure 12. The measurement was taken with the magnetic field parallel to the Si/dielectric interface normal

In Figure 14 we illustrate a cartoon figure of the K center, a silicon back bonded to three nitrogen atoms. Figure 15 illustrates a comparison between the normalized SDT intensities as a function of V_G (a) and the $\Delta J/J_0$ versus V_G (b) plot of figure 12. The normalization of figure 15 (a) is achieved by dividing the spin dependent modification to the tunneling current (I_{SDT}) by the total dc current (I). The I_{SDT}/I response very closely follows the characteristic trap assisted tunneling peak of figure 15(b), a very strong indication that we are observing spin dependent trap assisted tunneling current due to the defects largely responsible for the tunneling current.

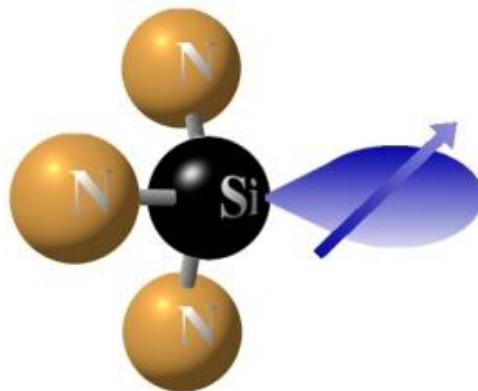


Figure 14: Schematic illustration of the K-center.

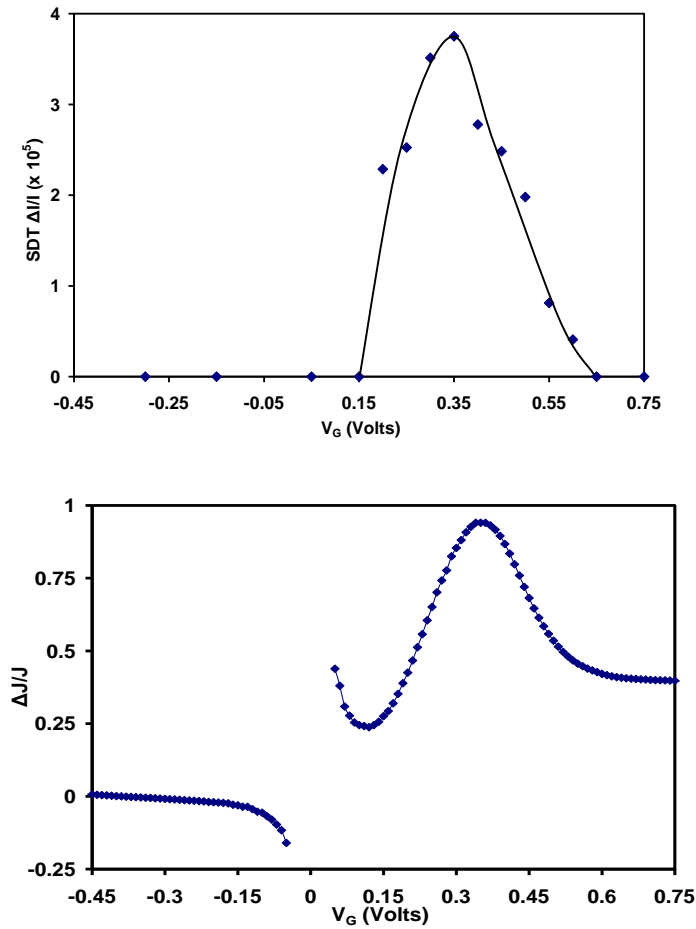


Figure 15: Comparison between SDT signal intensity ($\Delta I/I$) vs. V_G (a) and the $\Delta J/J$ vs. V_G curve (b) of figure 12. The SDT response ($\Delta I/I$) very closely follows the characteristic trap assisted tunneling peak of (b).

In an attempt to delineate between the spin dependent trap assisted tunneling current and the direct tunneling current, figure 16 shows the spin dependent modification to the tunneling current (I_{SDT}) as a function of V_G . It peaks at about 0.5 V, indicating that, as one would expect, the peak at $V_G = 0.35$ V in I_{SDT}/I of figure 15(a) is shifted downward because direct tunneling overwhelms the trap assisted tunneling process at higher bias. Since the direct tunneling is not spin dependent, the SDT response is not affected by the large direct tunneling current response which overwhelms the “electrically” measured trap assisted tunneling current at higher bias.

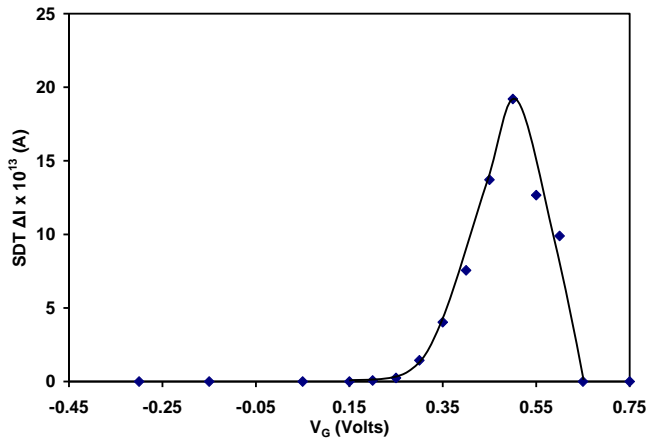


Figure 16: SDT spin dependent modification to the tunneling current I_{SDT} as a function of V_G . Note that it peaks at about $V_G = 0.5$ V indicating the peak at $V_G = 0.35$ V in the SDT I_{SDT}/I is shifted downward because direct tunneling overwhelms the trap assisted tunneling process at higher voltages

Figure 17 illustrates the poly-Si/SiO_xN_y/crystalline-Si (SOS) band diagram for three quite different biasing conditions: $V_G = 0$ V, 0.55 V, and 1.0 V. For simplicity of presentation, only two levels of a single dielectric trap are included in diagrams. These band diagrams were calculated using the Boise State University band diagram program.[30] Note first that there is very little band bending in the dielectric at any of the illustrated biasing levels. The dielectric is so thin that the relationship between the crystalline-Si/dielectric E_F and the defect energy level is nearly independent of the physical position of the defect with respect to the crystalline-Si/dielectric interface. This is so because of the enormous difference between the capacitance of the 1.2 nm EOT dielectric and the much thicker Si depletion region. Nearly all the voltage appears across the Si. Figure 16 shows that the SDT response appears at a V_G of about 0.2 V, peaks at 0.5 V, and has completely disappeared at about 0.65 V. At $V_G = 0.2$ V, where SDT appears, the crystalline-Si/dielectric E_F is 0.26 eV above the VBE. At $V_G = 0.65$ V, where the SDT disappears, the E_F is about 0.68 eV above the Si VBE. This narrow response must reflect a narrow distribution in K center levels.

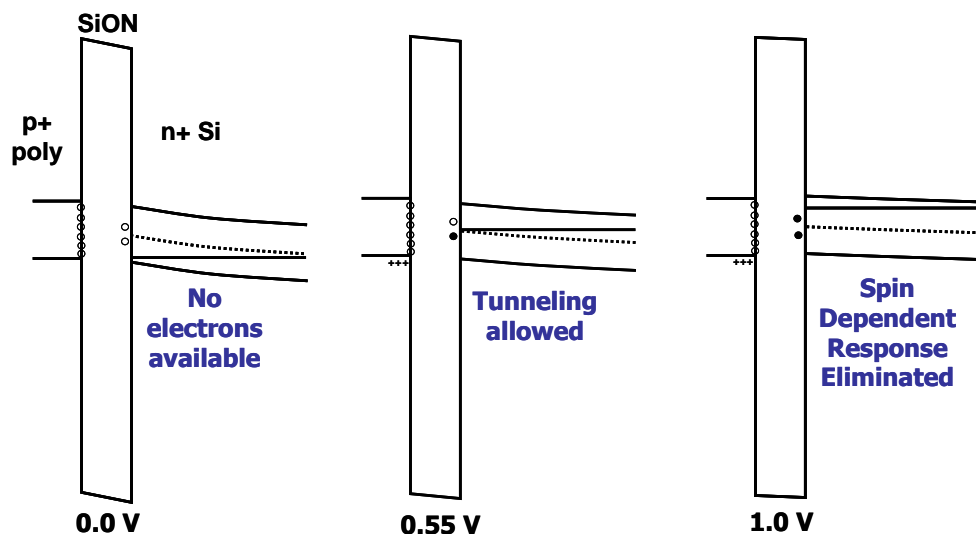


Figure 17: Energy band diagrams for the sample at three different values of V_G . Note that the only plausible explanation for the tunneling current must involve electron tunneling through defects with levels corresponding to the range of the silicon band gap. The simplified sketch illustrates two dielectric defect levels, consistent with experimental results.

An explanation of the response can be gleaned from a brief consideration of the physics of spin. The SDT process, like all EDMR processes, must involve a pair of spins initially separated physically. One of the spin sites is a K center. K centers, especially those nearest the crystalline-Si/dielectric boundary, can act like interface traps in that, as the E_F is advanced from the VBE toward the conduction band edge (CBE), the empty dangling bond trap levels (+/0) will accept an electron as the E_F crosses the relevant energy. This process is not spin dependent, whether or not it involves paramagnetism at the K center site, it does not involve paramagnetism from the valence band. However, once the K center is rendered paramagnetic, interactions of the K center site with another paramagnetic site would be spin dependent and thus susceptible to SDT. Should the K center accept an additional electron, it would be rendered diamagnetic again, insensitive to the SDT process.

Consider tunneling of an electron from a paramagnetic K center site to another paramagnetic site in the (highly defective) poly-Si gate. The process would be allowed only if the unpaired electron spins have opposite spin quantum numbers. If the two sites had electron spins with the same spin quantum number, the tunneling process would be forbidden Pauli exclusion principle. However, if the K center electron spin were to be “flipped” via EPR ($h\nu = g\beta H$) the previously forbidden tunneling event would be allowed. Thus, magnetic resonance could modulate such a tunneling process. The SDT process would thus “turn on” when E_F crosses the energy level corresponding to the first K center electron (+/0) transition which places one electron in the defect’s dangling bond orbital. Figure 18(a), a replotting of the results of figure 16 in which V_G is replaced by E_F , indicates that the SDT response begins to appear with E_F at about 0.26 eV above the VBE. The process peaks with E_F at about 0.54 eV.

Very crudely speaking, the energy range of 0.26 eV to 0.54 eV would correspond to the range of energy over which the K centers accept the first electron (+/0 transition). The SDT response drops from 0.54 eV to below our detection limit at 0.68 eV. So, to a rough approximation, the energy range of 0.54 eV – 0.68 eV corresponds to the range of energy over which the K centers accept the second electron (0/-) transition.

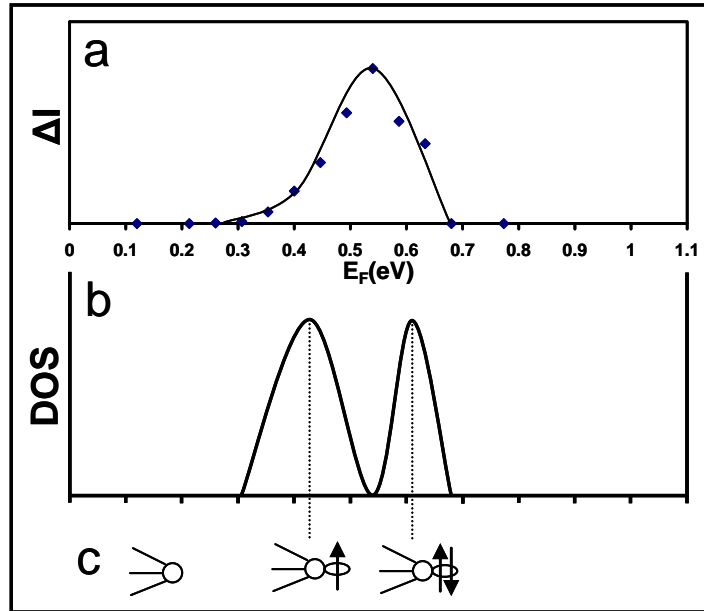


Figure 18: (a) The SDT response as a function of interface E_F , (b) a crude representation of K center density of states, and (c) a cartoon representation of the charge states of the K centers.

To a very crude approximation, we could approximate the collective K center density of states (DOS) by the absolute value of the derivative dI_{SDT}/dE_F . This is illustrated in figure 18(b). The cartoons of figure 18(c) illustrate the spin states (and charge) of the K centers versus E_F . We can understand how this is so by first considering an array of precisely identical defects which have precisely identical energy levels. Figure 19 (a) illustrates a more physically reasonable DOS in which each of the levels is broadened to take into account disorder. If the E_F is below the (+/0) level, the defect's unoccupied dangling bond orbital does not have an electron to contribute to the tunneling. The defect is also diamagnetic (no unpaired electron) and cannot take part in magnetic resonance. Thus, with E_F below the (+/0) level, no SDT signal can be observed.

However, if E_F crosses the (+/0) level of some of the K centers, these centers can contribute to the tunneling and are paramagnetic and do take part in magnetic resonance. Therefore, the SDT response begins to turn on as the E_F level crosses the lower (+/0) levels and increases as long as E_F continues to cross these levels. However, as the E_F begins to cross the (0/-) level, the orbitals begin to accept a second electron and become negative. When this happens, the centers lose their paramagnetism, because they are now occupied by two electrons of opposite spin, and can no longer take part in magnetic

resonance; thus, the SDT response is reduced. The SDT response drops to zero when all of the K centers accept the second electron. This SDT response is illustrated in figure 19(b).

Figure 19(c) illustrates the derivative of the SDT amplitude versus energy response of figure 19(b). Notice that the maximum on the left side of the trace occurs at the same energy as the (+/0) peak in figure 19(a). This is so because the increase in SDT amplitude versus energy will be greatest at the lower peak of the curve in figure 19(a). Analogously, since the rate of decrease in SDT amplitude versus energy will occur at the (0/+) peak, the minimum on the right will occur at that (0/+) energy. Thus, the absolute value of the derivative shown in figure 19(d) is a fairly good first order representation of the defect DOS illustrated in figure 19(a). It is important to point out that this absolute value of the derivative is only a first order representation of the actual DOS. If the (+/0) and (0/-) transition peaks overlap, the absolute value of the derivative will incorrectly indicate a zero in the DOS between the two peaks. Also, the tunneling transmission probability from the K centers to defects in the poly-Si gate will not be precisely constant throughout the energy range (about 0.4 eV) over which the SDT is observed. However, the transmission probability will vary relatively slowly over the energy range. Thus, although the experimental evaluation of the defects density of states is crude, it should still provide a reasonable measure of the (+/0) and (0/-) transition levels and thus the electron-electron correlation energy.

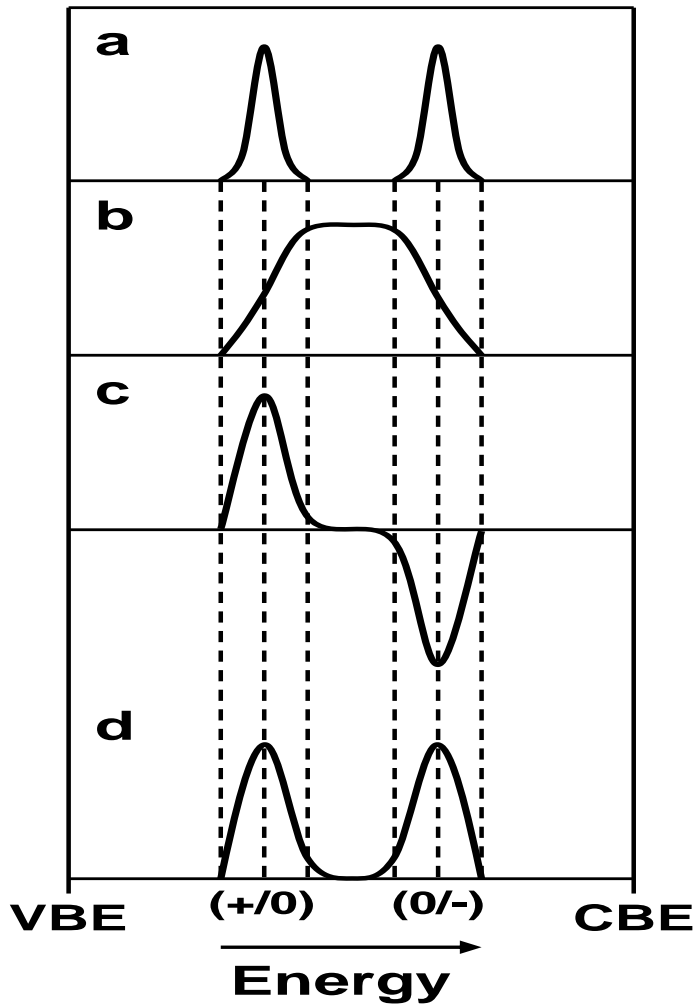


Figure 19: (a) A more physically reasonable DOS in which each of the levels is broadened to take into account disorder. (b) The SDT response from the levels of (a). (c) Schematic illustration of the derivative of the SDT amplitude vs. energy response of (b). (d) The absolute value of the derivative (c)

Conclusions

Two electrically detected magnetic resonance techniques have the sensitivity and analytical power to provide fundamental information about the physical and chemical nature of electrically active defects in fully processed solid state electronic devices of current technological interest. These techniques, in addition, can provide information about the spatial distribution and the energy levels of these defects.

References

1. J. A. Weil, J. R. Bolton, and J. E. Wertz, *Electron Paramagnetic Resonance: Elementary Theory and Practical Applications* (Wiley, New York, 1994.)
2. P. M. Lenahan and J. F. Conley, *J. Vac. Sci. Technol. B* **16**, 2134 (1998)
3. D. Kaplan, I. Solomon, and N. F. Mott, *J. Phys. (Paris) Lett.* **39**, 51 (1978)
4. D. J. Lepine, *Phys. Rev. B* **6**, 436 (1972)
5. P. M. Lenahan and M. A. Jupina, *Colloids Surf.* **45**, 191 (1990).
6. J. W. Gabrys, P. M. Lenahan, and W. Weber, *Microelectron. Eng.* **22**, 273
7. J. P. Campbell, P. M. Lenahan, A. T. Krishnan, and S. Krishnan, *J. Appl. Phys.* **103**, 044505 (2008)
8. J. P. Campbell, P. M. Lenahan, A. T. Krishnan, and S. Krishnan, *Appl. Phys. Lett.* **91**, 133507 (2007)
9. C.J. Cochrane, P.M. Lenahan, A.J. Lelis, to be published in *Journal of Applied Physics*
10. J.T. Ryan, P.M. Lenahan, A.T. Krishnan, and S. Krishnan, *Appl. Phys. Lett.* **96**, 223509 (2010)
11. J.T. Ryan, P.M. Lenahan, A.T. Krishnan, and S. Krishnan, *J. Appl. Phys.* **108**, 064511 (2010)
12. T. Grasser, W. Gos, V. Sverdlov, and B. Kaczer, *Proceedings of the IEEE International Reliability Physics Symposium*, 268 (2007)
13. D. J. Fitzgerald and A. S. Grove, *Surf. Sci.* **9**, 347 (1968)
14. E.H. Poindexter, P.J. Caplan, B.E. Deal, and R.R. Razouk, *J. Appl. Phys.* **52**, 879 (1981)
15. Y. Y. Kim and P. M. Lenahan, *J. Appl. Phys.* **64**, 3551 (1988)
16. A. Stesmans, B. Nouwen, and V.V. Afanas'ev, *Phys. Rev. B* **58**, 15801 (1998)
17. P. Campbell and P. M. Lenahan, *Appl. Phys. Lett.* **80**, 1945 (2002)
18. P. M. Lenahan and P. V. Dressendorfer, *Appl. Phys. Lett.* **41**, 542 (1982)
19. P. M. Lenahan and P. V. Dressendorfer, *J. Appl. Phys.* **55**, 3495 (1984)
20. G. J. Gerardi, E. H. Poindexter, P. J. Caplan, and N. M. Johnson, *Appl. Phys. Lett.* **49**, 348 (1986)
21. J.A. Cooper, *Phys. Status Solidi A* **162**, 305 (1997)
22. J.L. Cantin, H.J. Von Bardeleben, Y.S. Nisikin, Y.Re, R. P. Devaley, and W.J. Choyke, *Phys. Rev. Lett.* **92**, 015502 (2004)
23. E. Janzen, A. Gali, P. Carlsson, A. Gallstrom, B. Magnusson, and N.T. Son, *Physica* **B409**, 4354 (2009)
24. M. Bocksledte, A. Gali, A. Mattdusch, O. Pankratov, and J. W. Steeds, *Phys. Stat. Sol. B* **245**, 1281 (2001)
25. L.F. Register, E. Rosenbaum, and K. Yang, *Appl. Phys. Lett* **74**, 457 (1999)
26. E. Rosenbaum and L.F. Register, *IEEE Trans Electron Dev.* **44**, 317 (1997)
27. J. P. Campbell, P. M. Lenahan, A. T. Krishnan, and S. Krishnan, *J. Appl. Phys.* **103**, 044505 (2008)
28. D. T. Krick, P. M. Lenahan, and J. Kanicki, *J. Appl. Phys.* **64**, 3558 (1988)
29. W. L. Warren and P. M. Lenahan, *Phys. Rev. B* **42**, 1773 (1990)
30. R. G. Southwick and W. B. Knowlton, *IEEE Trans. Device Mater. Reliab.* **6**, 136(2006)